COMPUTED TOMOGRAPHY

Dual-energy-CT of hypervascular liver lesions in patients with HCC: investigation of image quality and sensitivity

Jens Altenbernd · Till A. Heusner · Adrian Ringelstein ·
Susanne C. Ladd · Michael Forsting · Gerald Antoch

Abstract
Objective To investigate dual-energy CT of hypervascular liver lesions in patients with HCC.
Methods Forty patients with hepatocellular carcinomas were investigated with abdominal dual-energy CT. In each patient unenhanced and contrast-enhanced imaging with arterial und portovenous delay were performed. Hypervascular lesions were documented on arterial phase 80-kVp images, 140-kVp images, and the averaged arterial images by two radiologists. Subjective image quality (5-point scale, from 5 [excellent] to 1 [not interpretable]) was rated on all images.
Results The mean number of hypervascular HCC lesions detected was 3.37 ± 1.28 on 80-kVp images ($p<0.05$), 1.43 ± 1.13 on 140-kVp images ($p<0.05$), and 2.57 ± 1.2 on averaged images. The image quality was 0.3 ± 0.5 for 80-kVp ($p<0.05$), 1.6 ± 0.5 for 140-kVp ($p<0.05$) and 3.2 ± 0.4 for the averaged images.
Conclusion Low-kVp images of dual-energy datasets are more sensitive in detecting hypervascular liver lesions. However, this increase in sensitivity goes along with a decrease in the subjective image quality of low-kVp images.

J. Altenbernd · T. A. Heusner · A. Ringelstein · S. C. Ladd ·
M. Forsting · G. Antoch
Department of Diagnostic and Interventional Radiology
and Neuroradiology, University Hospital Essen,
University of Duisburg-Essen,
Essen, Germany

J. Altenbernd (✉)
Department of Diagnostic and Interventional Radiology
and Neuroradiology, University Hospital Essen,
Hufelandstrasse 55,
45122 Essen, Germany
e-mail: jens.altenbernd@uk-essen.de

Introduction

A recent development in CT has been the introduction of dual-source technology [1]. On such CT systems, two X-ray tubes can be operated at different tube currents, making "dual-energy" imaging feasible. Dual-energy CT (DECT) implies simultaneous acquisition of datasets at two different photon spectra in a single CT examination [2] resulting in the ability to reconstruct the data at 80 kVp, 140 kVp, and at the weighted average. The weighted average dataset is a combination of image data from the 80- and 140-kVp datasets and can be used to generate a virtual 120-kVp dataset. In addition, virtual non-enhanced datasets can be reconstructed by using postprocessing algorithms [3].

One important advantage of dual-source CT compared with a single-source system is the option to use the two tubes at different tube currents offering differentiation of materials of non-equal radiographic density. The higher the difference in the two tube currents (e.g. 80 kVp and 140 kVp) used for imaging the better the differentiation between two materials of different density [2]. Based on these advantages potential applications of DECT when evaluating the abdomen are numerous [4]: Virtual non-enhanced images may be reconstructed from the existing datasets obviating the need for additional non-enhanced imaging. Consequently radiation exposure for the patient may be reduced. Furthermore, calcifications may be quantified and anatomical structures of high attenuation (such as the bone) can be removed semiautomatically.

Most HCCs are hypervascular lesions that typically enhance during the phase of maximum hepatic arterial

enhancement (the so-called hepatic arterial dominant phase) [5, 6]. Results of several studies have demonstrated that the use of a two-phase approach, with acquisition of images in the hepatic arterial dominant phase as well as in the portal venous phase, greatly improves the detection of HCC [5, 7–11]. Based on the fact that attenuation of iodine will be much greater at 80 kVp than at 140 kVp [12–18] we evaluated the clinical utility of DECT for detection of hypervascular lesions in hepatocellular carcinoma (HCC). Furthermore, virtual non-enhanced images were compared with "true" non-enhanced images.

Materials and methods

Patient population

Between April and August 2009, 40 consecutive patients (29 men, 11 women; mean age 64 years±10 years) underwent dual-energy CT (DECT) for evaluation of the liver for hypervascular lesions. This study was approved by our institutional review board and all patients provided written informed consent before participation.

CT protocol and effective radiation dose

All CT examinations were obtained using dual-source multi-detector CT (Somatom Definition™ Dual Source; Siemens Medical Solutions, Forchheim, Germany). This system consists of two x-ray tubes mounted on one gantry at a 90° angle [1] and two corresponding 64-section detectors. One detector (detector A) covers a 50-cm field of view and the other detector (detector B) covers a 26-cm field of view [1]. Patients were positioned supine on the table. Patients were positioned slightly off centre to the left to ensure complete coverage of the liver by the smaller field of view of detector B. First, unenhanced imaging of the abdomen was acquired from the dome of the liver to the iliac crest in an inspiratory breath hold by using a detector configuration of 64×0.6 mm, a tube current of 120 kVp, quality reference of 240 mAs, and online dose modulation [19]. With this vendor-specific software image noise characteristics are similar to those of CT images acquired at 240 mAs (effective) per section.

After intravenous injection of a non-ionic contrast agent (1.5 mL per kilogram of body weight, Xenetix 300™, *Guerbet, Sulzbach, Germany*) bolus tracking was started in the abdominal aorta at the level of the coeliac trunk with a threshhold of 120 HU. Dual-energy datasets were acquired in the arterial and portal venous (bolus tracking and 80 s) phases from the dome of the liver to the iliac crest by operating tube A at 140 kVp and a current effective value of 96 mAs and tube B at 80 kVp and a current effective

value of 404 mAs. For both tubes, an online dose modulation (Care DOSE 4D™, Siemens Medical Solutions) was used. For the dual-energy CT, collimation was set to 14×1.2 mm on both detectors. The single-energy unenhanced imaging was acquired with a pitch of 1.2 and the dual-energy imaging was acquired with a pitch of 0.55. For all imaging, the gantry rotation speed was 0.5 s. For each of the three phases, the dose-length product was recorded from the patient protocol. These values were used for calculation of an individual effective radiation dose by using appropriately normalised conversion factors (normalized to the body region-specific response to radiation) [20]. Effective radiation dose values in mSv were calculated for each phase. We compared the effective dose of a triple-phase protocol (true unenhanced and dual-energy in the arterial and portovenous phases) with that of a dual-phase protocol (dual-energy in arterial and portovenous phases) and calculated the percentage of dose reduction between those protocols.

Postprocessing and image reconstruction

Contiguous axial 3-mm true unenhanced and virtual unenhanced images were reconstructed. Axial post-contrast images were reconstructed by using a section thickness and an increment of 5 mm. The dual-energy CT generates three different series of images: 80-kV images, 140-kV images and weighted-average images, which are based on attenuation information on images obtained from both detectors, using 70% information from the high-keV and 30% from the low-keV imaging. Weighted-average images are similar to 120-kVp imaging of the abdomen and were used for measurements of contrast material uptake. Images were loaded onto a dedicated dual-energy post-processing workstation (syngo MMWP; Siemens Medical Solutions, Forchheim, Germany). Virtual unenhanced images can be reconstructed from the original dataset by subtracting iodine. This calculation is based on a so-called three-material decomposition: Assuming that every voxel in the abdomen is composed of fat, soft tissue and iodine, the algorithm generates a map that encodes the iodine distribution in each individual CT voxel. This map can subsequently be used to subtract iodine from the image, resulting in a virtual unenhanced image. To generate virtual unenhanced images, different values can be adjusted: the attenuation of fat and soft tissue at 80 and 140 kVp, an enhancement factor (relative contrast media, or Rel CM), the minimum and maximum attenuation in Hounsfield units and the number of adjacent voxels of the system that will be used for interpolation during the calculation of the three-material decomposition. For abdominal applications, standard soft tissue attenuations used by the system are 65 and 45 HU for 80 and 140 kVp, respectively, while typical values for fat are −110 and −95 HU, respectively.
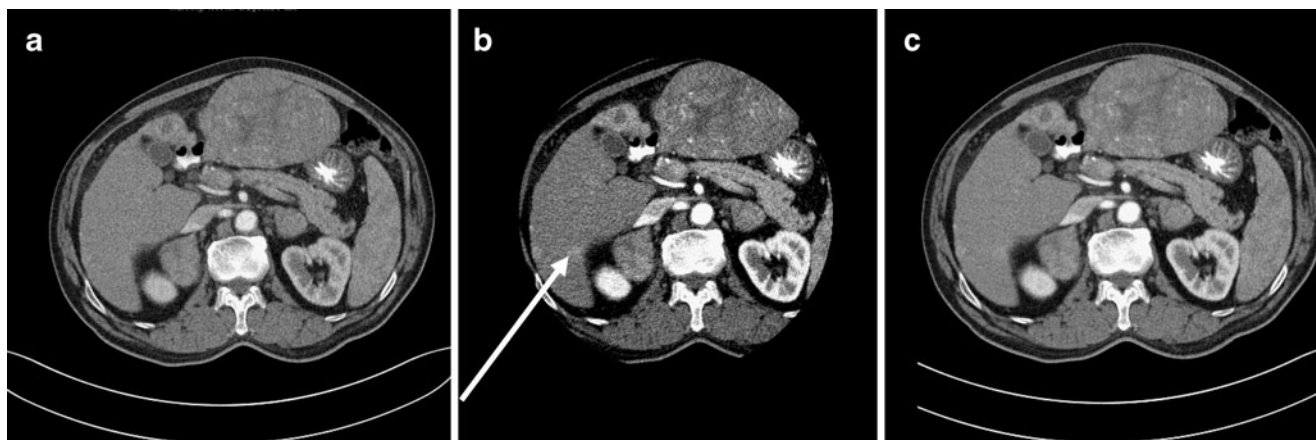
Fig. 1 Contrast-enhanced CT images obtained with a preset soft-tissue window (window width, 350 HU; window level, 50 HU) in a 64-year-old man with hepatocellular carcinoma. 140-kVp images (**a**), 80-kVp images (**b**) and averaged images (**c**) generated with dual-energy CT. 80-kVp images (**b**) show a hypervascular lesion, which is not identified on corresponding 140 kVp-images (**a**) and averaged images (**c**). There are other hypervascular liver lesions in the right and left lobe of the liver which also represent tumor

Image quality assessment

To quantify the percentage of the excluded parts of the liver, its diameter and the width of the parenchyma not included in the field of view of detector B were measured at the level of the liver hilum. Exclusion was classified as 0, none; 1, minimal (<25%); 2, mild (25–50%); 3, moderate (50–75%); and 4, severe (>75%). On both true unenhanced and virtual unenhanced images, CT attenuation was determined in six regions: normal hepatic parenchyma; aorta at the level of the coeliac trunk; psoas muscle; perihepatic fat; and air in front of the patient. In addition all hypervascular liver lesions were measured. All measurements were performed by the same physician (**BLINDED**), who had 9 years of experience in abdominal radiology, using regions of interest of 0.2–1.0 cm² in size. Tumour enhancement was defined as the difference between attenuation of a mass on contrast-enhanced images and its attenuation on either of the unenhanced images. For all measurements, the mean and standard deviations were calculated.

Qualitative analysis

Two experienced abdominal staff radiologists (**BLINDED**, with 9 years and 5 years of experience, respectively) in the interpretation of abdominal CT read all the cases together. On a dedicated workstation (syngo MMWP, Siemens Medical Solutions), 3-mm axial true unenhanced and virtual unenhanced images were displayed side by side. As images can be easily discriminated, radiologists were not blinded as to which image represented the true and virtual unenhanced dataset. Readers were asked to scroll through the sets of images and change window

and/or level settings according to their personal preference. For both image sets, the radiologists rated image noise on a five-point scale: 1, none; 2, minimal; 3, mild; 4, moderate; and 5, severe. Overall image quality was rated with a different five-point scale as follows: 5, excellent; 4, good; 3, fair; 2, poor; and 1, not interpretable. Furthermore, readers had to determine whether the limited field of view (26 cm) of detector B led to diagnostic limitations of the imaging. The readers were asked to determine whether the liver had undergone complete imaging. In addition, we sought to determine whether off-centre positioning of patients adversely affected the diagnostic quality of liver dual-energy CT. Both readers reported all hypervascular liver lesions separately for 80 kVp-, 140-kVp and averaged images within the postprocessing field of view (B-detector).

Statistical analysis

Attenuation of CT measured on true unenhanced and virtual unenhanced images were tested for differences by using the

Table 1 Attenuation values (HU) for 80-kVp, 140-kVp and averaged images in different anatomical regions of the abdomen

Anatomical region	80 kVp	140 kVp	Averaged images
HCC Lesion	119.3±33.5	77.5±16.6	91.7±21.3
Liver	69.8±10.6	57.2±7.2	60.4±7.4
Muscle	46.3±13.3	42.1±9.4	43.7±10.8
Fat	−109.5±16.3	−90.7±13.9	−87.6±15.9
Air	−957.6±141.4	−981.3±31.2	−972.3±96.3
Aorta	364.6±60.2	188.2±30.3	243.5±37.3

Table 2 Number of detected hypervascular lesions (HVL) for 80-kVp, 140-kVp and averaged images

Hypervascular lesion	80 kVp	140 kVp	Averaged images
HVL (mean per liver)	3.37±1.28	1.43±1.13	2.57±1.2
HVL (total number)	135	57	103

Wilcoxon test for paired samples. All calculations were performed by using statistical software (version 17; SPSS, IBM, Chicago, IL, USA). Means and standard deviations were calculated for each image quality category. Effective radiation doses for two-phase and three-phase protocols were calculated, and results were tested for statistical significance by using the Wilcoxon test.

Results

Lesion attenuation and detection

The mean attenuation values of 80 kVp- and 140 kVp images for hypervascular hepatic lesions in the arterial phase were 119.3±33.5 HU and 77.5±16.6 HU, respectively. On averaged images attenuation was 91.7±21.3 HU. This was significantly different from 80-kVp- and 140-kVp images (p <0.001 for both comparisons, Fig. 1). All other anatomical regions (liver, fat, aorta, muscle, air) differed significantly when the three datasets were compared (Table 1).

The number of detected lesions on 80-kVp, 140-kVp and averaged images was 3.4±1.3, 1.4±1.1, and 2.6±1.2, respectively. These differences were significant (Table 2).

Virtual and true unenhanced images

The attenuation values on true unenhanced and virtual unenhanced datasets of muscle and aorta were similar while values of hypervascular liver lesions, liver parenchyma and fat differed significantly when comparing attenuation values on virtual and true unenhanced scans (Table 3, Fig. 2).

Liver delineation

In 25 examinations the liver underwent complete imaging with the 26-cm field-of-view detector; in 15 examinations liver coverage was incomplete. Potential incomplete coverage of liver parenchyma with the 26-cm field-of-view detector was rated as 0.58±0.59 (range, 0–2; SD, 0.59) on the five-point scale.

Patient dose and image noise

The mean effective dose of the true unenhanced images was 3.88 mSv±1.77 (min. 2.1 mSv, max 5.8 mSv). The mean effective dose of the arterial und portal venous imaging together was 4.5 mSv ± 1.89 (min. 2.5 mSv, max. 7.8 mSv).

The mean overall image noise was rated as moderate (2.0±0.8) on virtual unenhanced images and as minimal (1.1±0.73) on true unenhanced images (p<.0001), while overall image quality was rated as good (1.5±0.54) and excellent (3.8±0.46), respectively (p<.001). The background noise, subjective noise rating, signal-to-noise ratio, contrast-to-noise ratio, lesion-to-liver ratio and image quality on 80-kVp, 140-kVp and averaged images are summarised in Table 4.

Discussion

This study demonstrates the feasibility of contrast-enhanced dual-energy CT for detection of hypervascular liver lesions in patients with hepatocellular carcinoma. Higher detection rates are based on higher attenuation of iodine in the low-kVp images in comparison to 140-kVp and averaged 120-kVp equivalent images. Hypervascular liver lesions had significantly higher attenuation values on 80-kV images than on averaged and 140-kVp images which correlates with the results of other studies [21, 22]. This also leads to a higher lesion-to-liver ratio. Because there is increased photoelectric absorption at 80 kVp relative to the absorption at 140 kVp and 120 kVp, contrast material has higher attenuation at lower peak voltage. This ultimately may enable better depiction of small lesions or, alternatively, a smaller amount of contrast material to be injected at similar detection rates [21]. Our data are supported by the findings of Nakayama et

Table 3 Attenuation values (HU) for true unenhanced and virtual unenhanced images in different anatomical regions of the abdomen

Variable	HCC lesion	Liver	Muscle	Fat	Aorta
True un-enhanced[a]	45.9±8.5	50.8±7.4	41.4±10	−99±12.6	36.8±6.4
Virtual un-enhanced[a]	48.4±9.2	54.1±7.4	42.8±9.8	−87.7±15	37.1±7.1
p value	0.015	0.000	0.519	0.000	0.88

[a] Data are mean attenuation values±standard deviations

Fig. 2 True unenhanced (**a**) and virtual unenhanced (**b**) images in a 55-year-old male patient. Note the differences in density of the spleen on virtual unenhanced images (**b**) caused by the smaller field-of-view of detector B
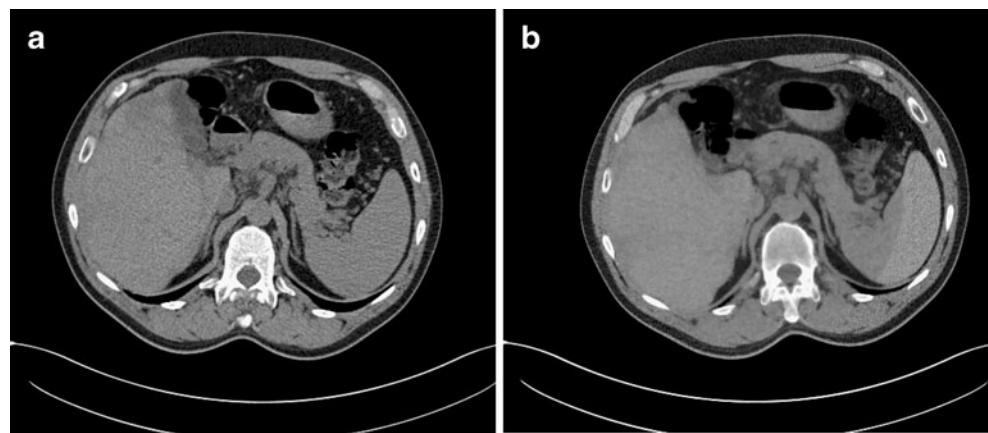
al. who reported that the amount of contrast material can be reduced by at least 20% without degradation in image quality when reducing the tube voltage from 120 kV to 90 kV [23]. In addition, in this study imaging obtained with low tube voltage led to a reduction in radiation dose by as much as 57%. Decreasing the tube voltage and the iodine concentration of the contrast material particularly would benefit patients who may need to undergo multiple CT examinations, young patients who are at increased risk of developing cancer from medical radiation exposure [24], or those patients with renal impairment.

The acquisition of dual-energy datasets enables the reconstruction of virtual unenhanced images, on which the iodine content of contrast-enhanced images has been subtracted [1–3, 22]. This dual-energy technique is based on the varying attenuation of different materials at different CT energies. These differences are caused by material-dependent Compton and photoelectric effects [25]. The differences between the mean attenuation values of different anatomical structures on virtual unenhanced and true unenhanced images were significant. However, in our opinion the differences shown in Table 3 may be considered clinically insignificant. Other studies have shown a good correlation between the true and virtual unenhanced images [4, 26].

There is a great potential of dual-energy CT for dose reduction compared with conventional multi-detector CT.

Our data suggest that replacement of true unenhanced images by virtual unenhanced images would lead to dose reduction of 30% for the liver protocol. In particular young patients or those with benign or potentially curable malignant disease would benefit from a reduced dose. Other studies have shown that virtual unenhanced images have diagnostic accuracy equal to that of true unenhanced images [21, 22, 27].

Although the image quality of 80-kVp, 140-kVp and averaged images differs significantly when assessed qualitatively, there was no statistical difference in contrast-to-noise and signal-to-noise ratios between 80-kVp and averaged images. However, between 80-kVp and 140-kVp images differences in qualitative assessment of image quality were significant. An increase in image noise may not represent a clinical problem for the detection of hypervascular liver lesions due to a high lesion-to-liver ratio, but it remains to be determined whether higher noise will adversely affect the interpretation of other anatomical or pathological phenomena in the upper abdomen. An option would be specific techniques to reduce image noise in the setting of low kVp images. Kalra et al. reported on noise reduction filters that effectively helped to reduce the noise on CT images acquired with a radiation dose reduced by 50% without compromising image quality. Their filters were developed to compensate for the degradation of image quality that results from the increased noise that accompanies the use of reduced tube current [28–30].

This study is not without limitations. Histopathology was not available for hypervascular lesions detected with CT imagingThe clinical relevance of hypervascular lesions detected on 80 kVp images will have to be evaluated in future studies. In addition, the small field of view of the B detector sometimes leads to incomplete display of the liver parenchyma. Usually a left-centred position of the patient on the examination table can compensate for this limitation but has to be considered before starting the CT [26]. Another problem refers to image reconstruction in those datasets with incomplete coverage of the liver and upper

Table 4 Image quality parameters for 80-kVp, 140-kVp and averaged images

Variable	80 kVp	140 kVp	Averaged images
BN	12.3±3.5	9.4±3.4	7.7±2.4
Subjective noise rating	4.1±1.3	2.3±2.1	2.5±0.5
SNR	10.2±5.1	8.7±4.3	12.5±4.7
CNR	6.4±3.6	4.7±2.5	6.9±3.4
LLR	1.7±0.5	1.4±0.3	1.5±0.4
Image quality	0.3±0.5	1.6±0.5	3.2±0.4

abdomen. In these cases all data outside the 80-kVp / 26-cm tube field-of-view are reconstructed based on only the 140-kVp tube field-of-view leading to inconsistency in the reconstructed image. This problem will be solved by including two tubes with a large field-of-view as can be found with currently available top-of-the-line dual-energy imaging systems. Thus, the new generation of CT has an expanded B detector (42 cm), which is indispensable for implementation of dual-energy technology in daily routine.

References

1. Flohr TG, Mccollough CH, Bruder H et al (2006) First performance evaluation of a dual-source CT (DSCT) system. Eur Radiol 16:256–268
2. Johnson TR, Krauss B, Sedlmair M et al (2007) Material differentiation by dual energy CT: initial experience. Eur Radiol 17:1510–1517
3. Scheffel H, Stolzmann P, Frauenfelder T et al (2007) Dual-energy contrast-enhanced computed tomography for the detection of urinary stone disease. Invest Radiol 42:823–829
4. Graser A, Johnson TR, Chandarana H et al (2009) Dual energy CT: preliminary observations and potential clinical applications in the abdomen. Eur Radiol 19:13–23
5. Baron RL, Oliver JH 3rd, Dodd GD 3rd et al (1996) Hepatocellular carcinoma: evaluation with biphasic, contrast-enhanced, helical CT. Radiology 199:505–511
6. Oliver JH 3rd, Baron RL (1996) Helical biphasic contrast-enhanced CT of the liver: technique, indications, interpretation, and pitfalls. Radiology 201:1–14
7. Oliver JH 3rd, Baron RL, Federle MP et al (1996) Detecting hepatocellular carcinoma: value of unenhanced or arterial phase CT imaging or both used in conjunction with conventional portal venous phase contrast-enhanced CT imaging. AJR Am J Roentgenol 167:71–77
8. Ohashi I, Hanafusa K, Yoshida T (1993) Small hepatocellular carcinomas: two-phase dynamic incremental CT in detection and evaluation. Radiology 189:851–855
9. Hollett MD, Jeffrey RB Jr, Nino-Murcia M et al (1995) Dual-phase helical CT of the liver: value of arterial phase scans in the detection of small (< or = 1.5 cm) malignant hepatic neoplasms. AJR Am J Roentgenol 164:879–884
10. Oliver JH 3rd, Baron RL, Federle MP et al (1997) Hypervascular liver metastases: do unenhanced and hepatic arterial phase CT images affect tumor detection? Radiology 205:709–715
11. Paulson EK, Mcdermott VG, Keogan MT et al (1998) Carcinoid metastases to the liver: role of triple-phase helical CT. Radiology 206:143–150
12. Huda W (2002) Dose and image quality in CT. Pediatr Radiol 32:709–713, discussion 751-704
13. Kalva SP, Sahani DV, Hahn PF et al (2006) Using the K-edge to improve contrast conspicuity and to lower radiation dose with a 16-MDCT: a phantom and human study. J Comput Assist Tomogr 30:391–397
14. Sahani DV, Kalva SP, Hahn PF et al (2007) 16-MDCT angiography in living kidney donors at various tube potentials: impact on image quality and radiation dose. AJR Am J Roentgenol 188:115–120
15. Schueller-Weidekamm C, Schaefer-Prokop CM, Weber M et al (2006) CT angiography of pulmonary arteries to detect pulmonary embolism: improvement of vascular enhancement with low kilovoltage settings. Radiology 241:899–907
16. Heyer CM, Mohr PS, Lemburg SP et al (2007) Image quality and radiation exposure at pulmonary CT angiography with 100- or 120-kVp protocol: prospective randomized study. Radiology 245:577–583
17. Sigal-Cinqualbre AB, Hennequin R, Abada HT et al (2004) Low-kilovoltage multi-detector row chest CT in adults: feasibility and effect on image quality and iodine dose. Radiology 231:169–174
18. Waaijer A, Prokop M, Velthuis BK et al (2007) Circle of Willis at CT angiography: dose reduction and image quality–reducing tube voltage and increasing tube current settings. Radiology 242:832–839
19. Graser A, Wintersperger BJ, Suess C et al (2006) Dose reduction and image quality in MDCT colonography using tube current modulation. AJR Am J Roentgenol 187:695–701
20. Bongartz G, Golding SJ, Jurik AG, European, Computed Gfm, Tomography et al (2004) European guidelines for multislice computed tomography. European Commission, Brussels
21. Chandarana H, Godoy MC, Vlahos I et al (2008) Abdominal aorta: evaluation with dual-source dual-energy multidetector CT after endovascular repair of aneurysms—initial observations. Radiology 249:692–700
22. Stolzmann P, Frauenfelder T, Pfammatter T et al (2008) Endoleaks after endovascular abdominal aortic aneurysm repair: detection with dual-energy dual-source CT. Radiology 249:682–691
23. Nakayama Y, Awai K, Funama Y et al (2005) Abdominal CT with low tube voltage: preliminary observations about radiation dose, contrast enhancement, image quality, and noise. Radiology 237:945–951
24. Brenner D, Elliston C, Hall E et al (2001) Estimated risks of radiation-induced fatal cancer from pediatric CT. AJR Am J Roentgenol 176:289–296
25. Avrin DE, Macovski A, Zatz LE (1978) Clinical application of Compton and photo-electric reconstruction in computed tomography: preliminary results. Invest Radiol 13:217–222
26. Graser A, Johnson TR, Hecht EM et al (2009) Dual-energy CT in patients suspected of having renal masses: can virtual non-enhanced images replace true nonenhanced images? Radiology
27. Chae EJ, Song JW, Seo JB et al (2008) Clinical utility of dual-energy CT in the evaluation of solitary pulmonary nodules: initial experience. Radiology 249:671–681
28. Kalra MK, Maher MM, Blake MA et al (2004) Detection and characterization of lesions on low-radiation-dose abdominal CT images postprocessed with noise reduction filters. Radiology 232:791–797
29. Kalra MK, Maher MM, Sahani DV et al (2003) Low-dose CT of the abdomen: evaluation of image improvement with use of noise reduction filters pilot study. Radiology 228:251–256
30. Kalra MK, Wittram C, Maher MM et al (2003) Can noise reduction filters improve low-radiation-dose chest CT images? Pilot study. Radiology 228:257–264